

Supporting Information

CH₄ storage and CO₂ capture in highly porous zirconium oxide based metal-organic frameworks

Qingyuan Yang,^{a,b} Vincent Guillerm,^c Florence Ragon,^c Andrew D. Wiersum,^d Philip L. Llewellyn,^d

Chongli Zhong,^a Thomas Devic,^c Christian Serre,^c Guillaume Maurin^{b*}

^a State Key Laboratory of Organic-Inorganic Composites, Beijing University of Chemical Technology, Beijing 100029, China.

^b Institut Charles Gerhardt Montpellier, UMR CNRS 5253, UM2, ENSCM, Place E. Bataillon, 34095 Montpellier cedex 05 France

^c Institut Lavoisier, UMR CNRS 8180-Université de Versailles St Quentin en Yvelines, 45 avenue des Etats-Unis, 78035 Versailles, France

^d Laboratoire Chimie Provence, Universités Aix-Marseille I, II et III - CNRS, UMR 6264, Centre de Saint Jérôme, 13397 Marseille, France

1. Synthesis

Ligand 4,4'-azobenzenedicarboxylic acid (AzoBDC)

This was prepared following an already described synthetic procedure^{1a,1b} also employed in a recent study for the preparation of the Zr₆-AzoBDC^{1c}. 90 mmol (15 g) of 4-nitro-2-chlorobenzoic acid (Sigma Aldrich, 97%) and 1250 mmol (50 g) of sodium hydroxide (Alfa Aesar, 98%) were dispersed in about 120 mL of distilled water, and heated at 50-60 °C under magnetic stirring until the complete dissolution of the solid. 555 mmol (100 g) of glucose (Sigma Aldrich, 96%) dissolved in 150 mL of hot distilled water were added slowly to the previous mixture. The solution turned from yellow to orange and then dark brown. After 10 minutes, the heating was stopped and air was bubbled through the solution for 4-5 hours at room temperature. The mixture was cooled down with an ice bath; the disodium salt was recovered by filtration, washed with minor amount of ethanol and re-dissolved at room temperature in about 100 mL of distilled water. Hydrochloric acid (VWR 37%) was added under stirring until the pH reached 1, a pink precipitate was obtained. The mixture was stirred for few hours, and then the solid was again recovered by filtration, washed with ethanol and dried under vacuum at 50 °C.

The characterization of this ligand can be found in the previous studies^{1b,1c}.

Ligand 3,3'-dichloro-4,4'-azobenzenedicarboxylic acid (Cl₂AzoBDC)

This was prepared following a modified procedure^{1a}.

74 mmol (15 g) of 4-nitro-2-chlorobenzoic acid (Sigma Aldrich, 97%) and 1250 mmol (50 g) of sodium hydroxide (Alfa Aesar, 98%) were dispersed in about 120 mL of distilled water, and heated at 50-60 °C under magnetic stirring until the complete dissolution of the solid. 555 mmol (100 g) of glucose (Sigma Aldrich, 96%) dissolved in 150 mL of hot distilled water were added slowly to the previous mixture. The solution turned from yellow to orange and then dark brown. After 10 minutes, the heating was stopped and air was bubbled through the solution for 4-5 hours at room temperature. The mixture was cooled down with an ice bath; the disodium salt was recovered by filtration, washed with minor amount of ethanol and re-dissolved at room temperature in about 100 mL of distilled water. Hydrochloric acid

(VWR 37%) was added under stirring until the pH reached 1, a pink precipitate was obtained. The mixture was stirred for few hours, and then the solid was again recovered by filtration, washed with ethanol and dried under vacuum at 50 °C.

NMR ^1H ($\text{d}_6\text{-DMSO}$): 12-13 (broad, 2H), 8.03 (d, $J_1 = 8.1$ Hz, 4H), 8.03 (d, $J_2 = 1.5$ Hz, 4H); 7.97 (dd, $J_1 = 8.1$ Hz, $J_2 = 1.5$ Hz, 4H).

NMR ^{13}C ($\text{d}_6\text{-DMSO}$): 166.2, 153.1, 134.1, 132.7, 131.9, 124.0, 122.1.

IR data, ν (cm^{-1}): 3495 (b), 1687 (s), 1589 (m), 1561(w), 1476 (m), 1410 (m), 1384 (m), 1263(s), 1041(m), 912 (w), 893 (m), 847 (m).

Extended UiO-66 MOFs

Optimized solvothermal syntheses general protocol of **UiO-66** or $\text{Zr}_6\text{O}_4(\text{OH})_4[\text{O}_2\text{C-C}_6\text{H}_4\text{-CO}_2]$, **UiO-67** or $\text{Zr}_6\text{O}_4(\text{OH})_4[\text{O}_2\text{C-C}_{12}\text{H}_8\text{-CO}_2]$, **Zr₆-AzoBDC** or $\text{Zr}_6\text{O}_4(\text{OH})_4[\text{O}_2\text{C-C}_{12}\text{H}_8\text{N}_2\text{-CO}_2]$ and **Zr₆-Cl₂AzoBDC** or $\text{Zr}_6\text{O}_4(\text{OH})_4[\text{O}_2\text{C-C}_{12}\text{H}_6\text{N}_2\text{Cl}_2\text{-CO}_2]$ follows the same general procedure.

The ligand and 0.5 mmol of ZrCl_4 (Alfa Aesar, 99.5+%) were introduced in a 23mL Teflon-lined steel autoclave. DMF was added, the mixture stirred for few minutes at room temperature, the autoclave sealed, placed in an oven. Please refer to Table S1 for amount of ligand, DMF, synthesis time and temperature.

Table S1. Synthesis conditions of the extended UiO-66 solids.

Phase	Ligand	n_{ligand} (mmol)	Metal precursor	n_{metal} (mmol)	V_{DMF} (mL)	HCl (mmol)	Time (h)	T (°C)	Yield (%)*)
UiO-66	BDC	0.5	ZrCl_4	0.5	5.0	1.0	16	220	95
UiO-67	4,4'-BPDC	0.5	ZrCl_4	0.5	3.0	1.0	24	150	92
Zr₆-AzoBDC	AzoBDC	0.75	ZrCl_4	0.5	5.0	1.0	60	100	-
Zr₆-Cl₂AzoBDC	Cl ₂ AzoBDC	0.75	ZrCl_4	0.5	5.0	1.0	60	100	87

(*) based on zirconium

Typically, the MOFs were activated through soaking in DMF overnight at room temperature, followed by soaking in MeOH or THF overnight at room temperature, before evacuation at 150 °C.

2. Determination of the experimental unit cell parameters from X-ray powder diffraction)

If all XRPD could be successfully indexed using the dicvol software in the cubic space groups, one had to consider the symmetry of the organic spacer to determine which space group would be adequate for each sample. Thus, as one can see Fig. S1, that some linkers possess only an inversion center or a symmetry axis (Note that BPDC phenyl rings can rotate which rules out the presence of the inversion centre for UiO-67). Finally, the presence of additional but weak peaks deduced from Synchrotron XRPD allowed to choose between the different space groups, which explain why Zr₆-AzoBDC and Zr₆-Cl₂AzoBDC correspond to Fm-3 SG.

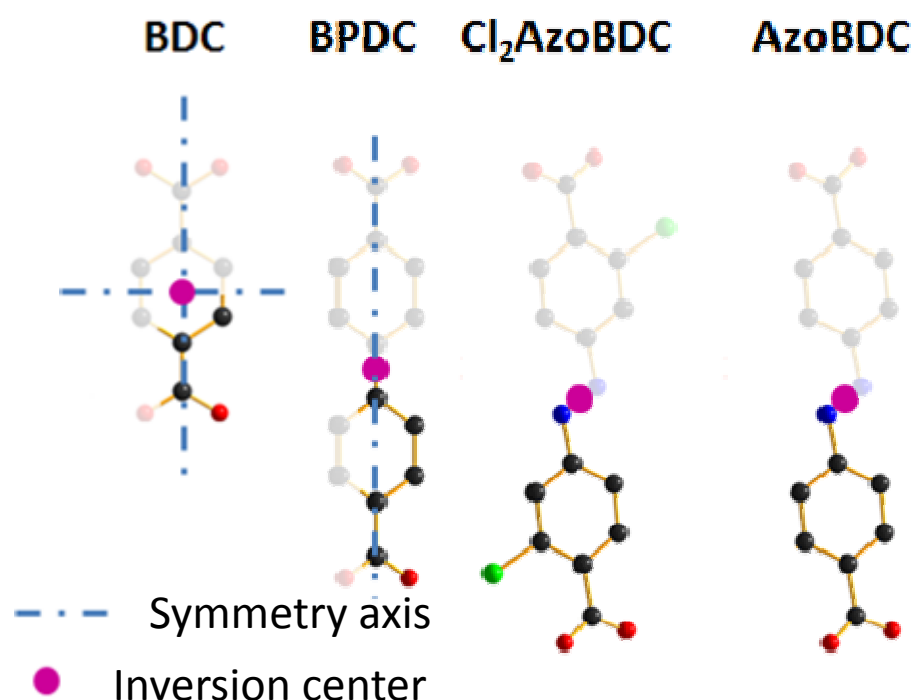


Fig. S1. Symmetry considerations used to determine the space groups of the series of *UiO* derivatives.

Pattern matching of the extended UiO solids

The structures of extended UiO materials (UiO-67, Zr₆Cl₂AzoBDC, Zr₆AzoBDC) were simulated using computer modeling based on experimental cell parameters. Their powder patterns were indexed using Dicvol and then refined using Fullprof and its graphical interface Winplotr ([Error! Reference source not found.](#) to [Error! Reference source not found.](#)).

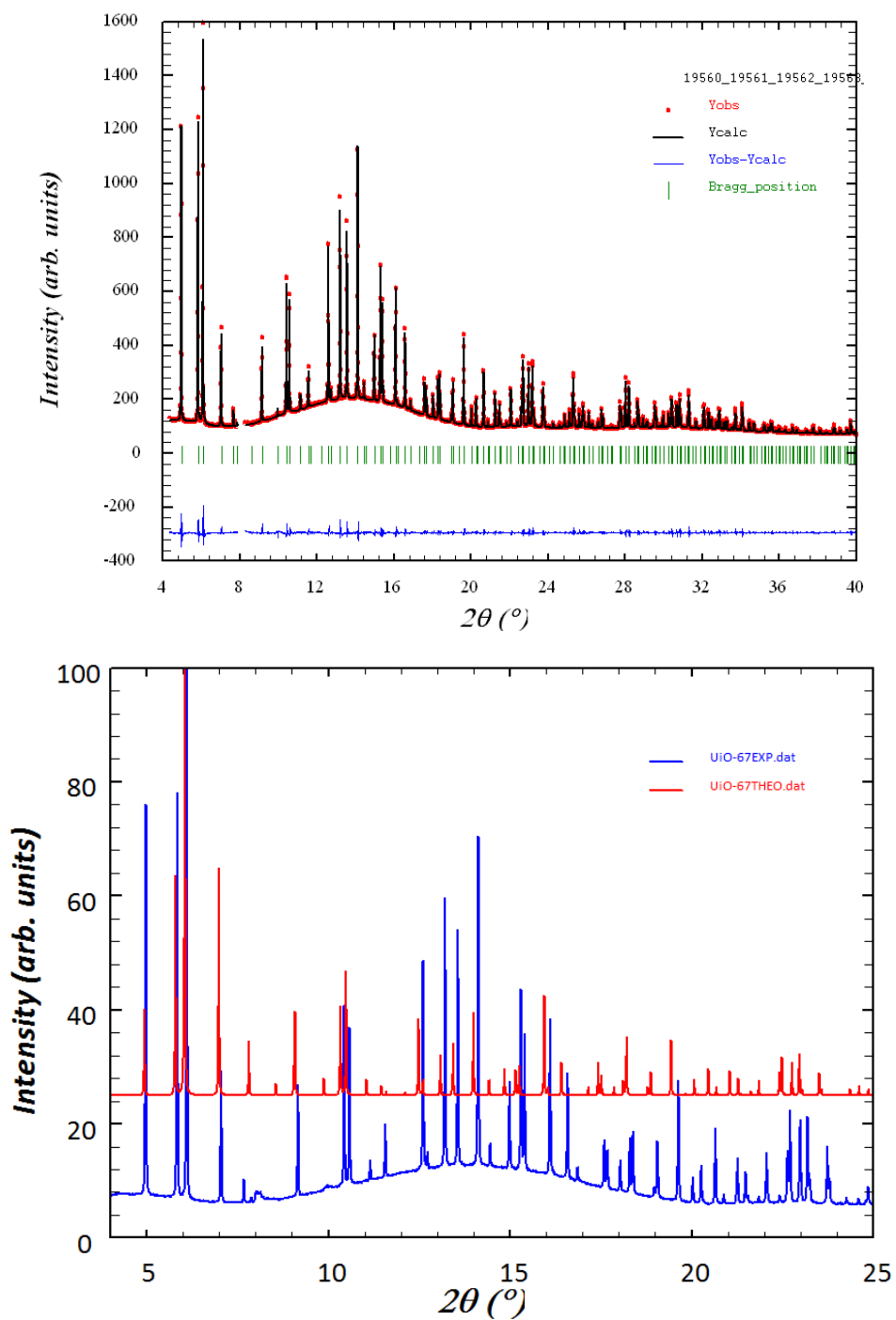


Fig. S2. Top: structureless pattern profile refinement plot of UiO-67 . Excluded area corresponds to an artifact from the beamline. Bottom: Superposition of experimental and calculated (from the DFT optimized structures) diffractograms ($\lambda \sim 0.82639 \text{\AA}$).

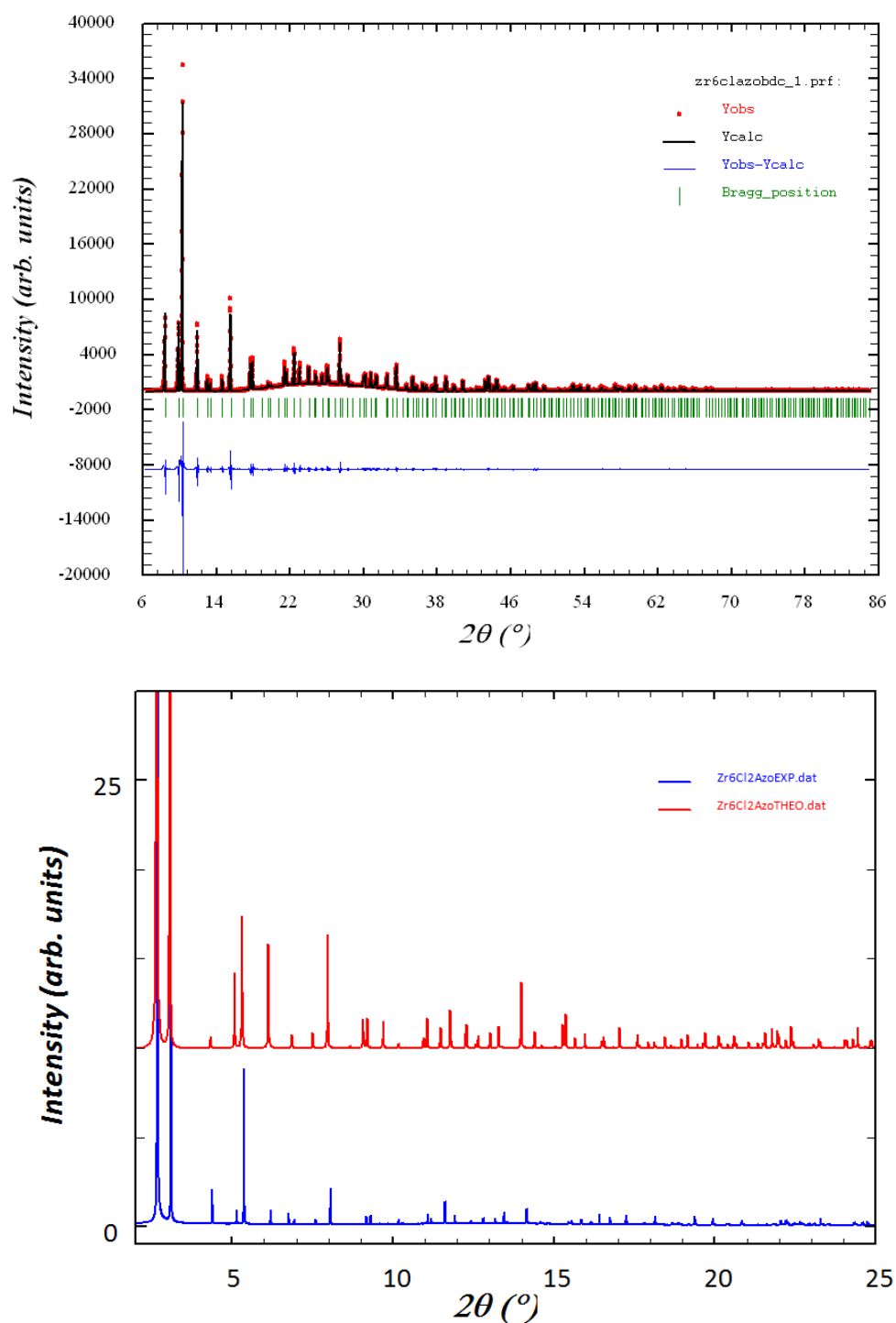


Fig. S3. Top: structureless pattern profile refinement plot of $\text{Zr}_6\text{-Cl}_2\text{AzoBDC}$. Bottom: Superposition of experimental and calculated (from the DFT optimized structures) diffractograms ($\lambda \sim 0.799910 \text{ \AA}$).

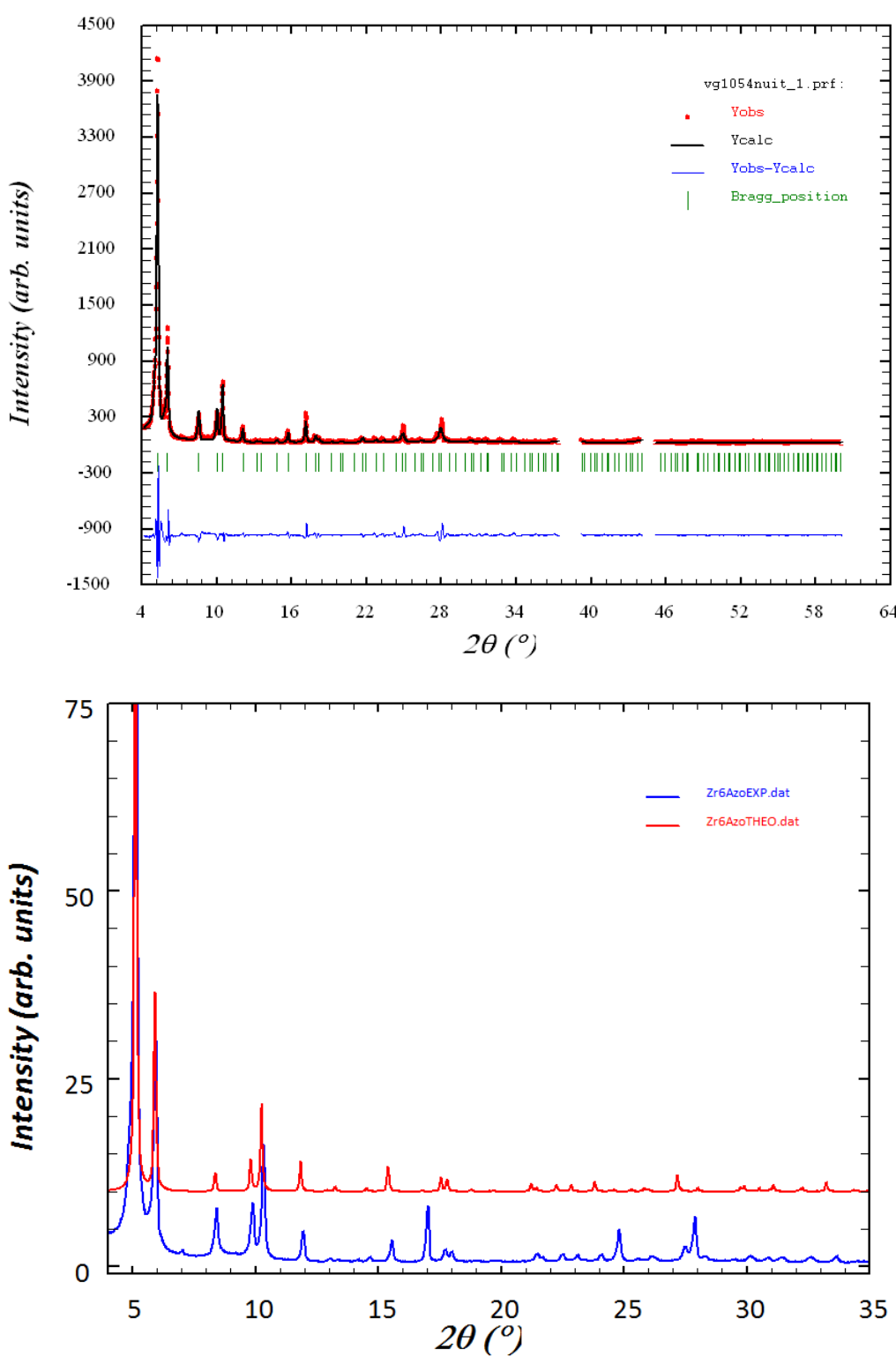


Fig. S4. Top: structureless pattern profile refinement plot of Zr_6AzoBDC . Excluded areas correspond to peaks from the aluminum sample holder. Bottom: superposition of experimental and calculated (from the DFT optimized structures) diffractograms ($\lambda_{\text{Cu}} \sim 1.54056 \text{\AA}$).

3. Thermal behavior

X-ray thermodiffractometry and thermogravimetric analysis of the UiO-66s.

The X-Ray Thermodiffractometers for UiO-66, UiO-67, Zr₆-AzoBDC and Zr₆-Cl₂AzoBDC have been collected (**Error! Reference source not found.** and Table S2).

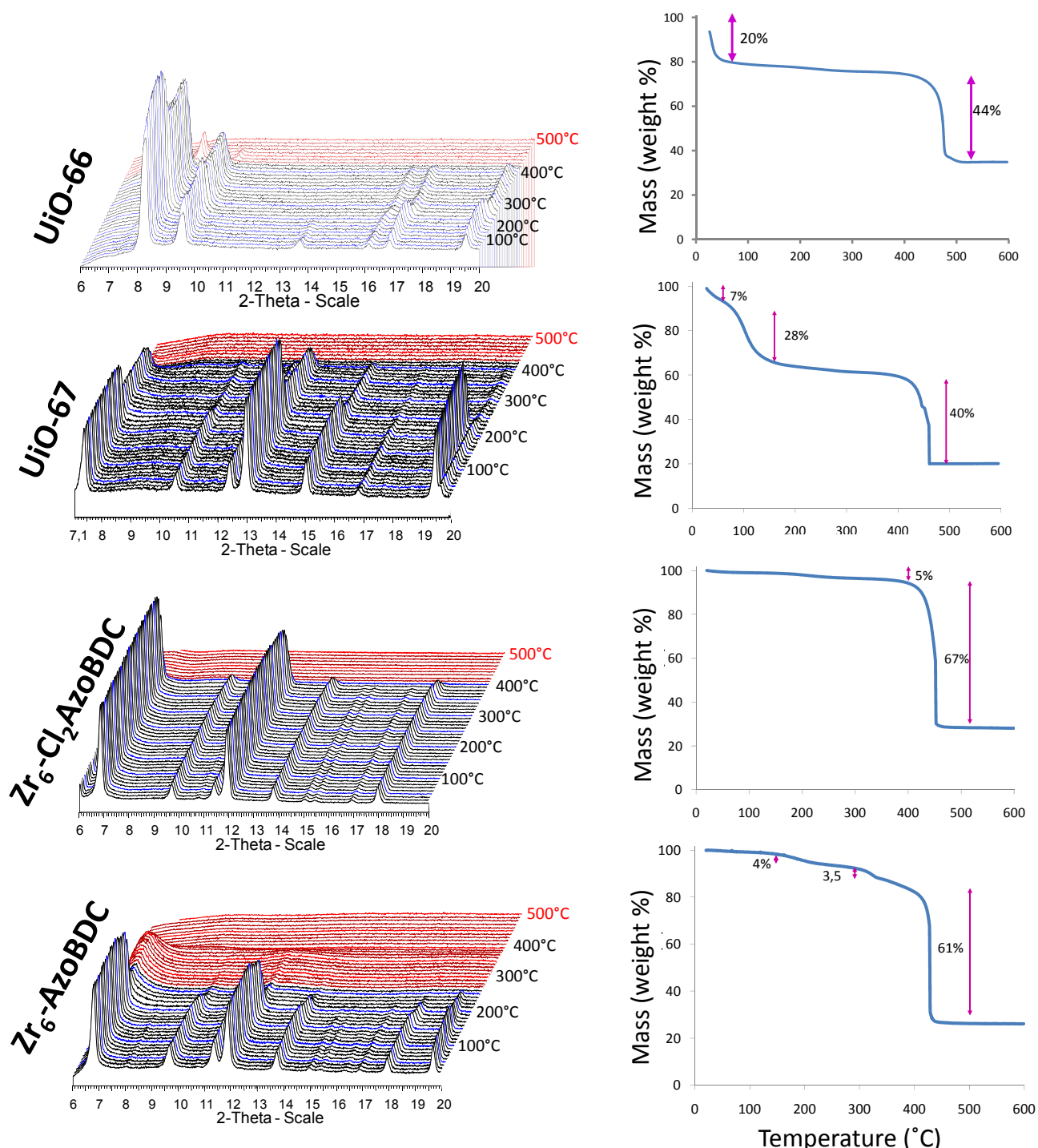


Fig. S5. X-Ray Thermodiffractometry (left) ($\lambda_{Co}=1.7906\text{\AA}$) and TGA (right) under air of UiO solids built up from 1,4-BDC, 4,4' BPDC, 3,3',4,4'-Cl₂AzoBDC and 4,4'-AzoBDC (top to bottom).

Table S2. Comparison of the experimental and theoretical weight losses for the UiO solids.

	Theoretical weight loss (%)	Experimental weight loss (%)
UiO-66	45	44
UiO-67	58	60
Zr₆-AzoBDC	60	61
Zr₆-Cl₂AzoBDC	69	67

4. Stability upon water adsorption

The water tolerance of UiO-66, UiO-67 and Zr₆-Cl₂AzoBDC has been checked (Fig. S6). Typically, 100 mg of material has been soaked in 5 mL of water under magnetic stirring for 24 hours. The powder was then recovered by filtration and the crystallinity checked by XRD. Please note that the low quality for the Zr₆-Cl₂AzoBDC is due to the small amount of the product which was recovered. Nevertheless, the diagrams clearly show that the structure is conserved.

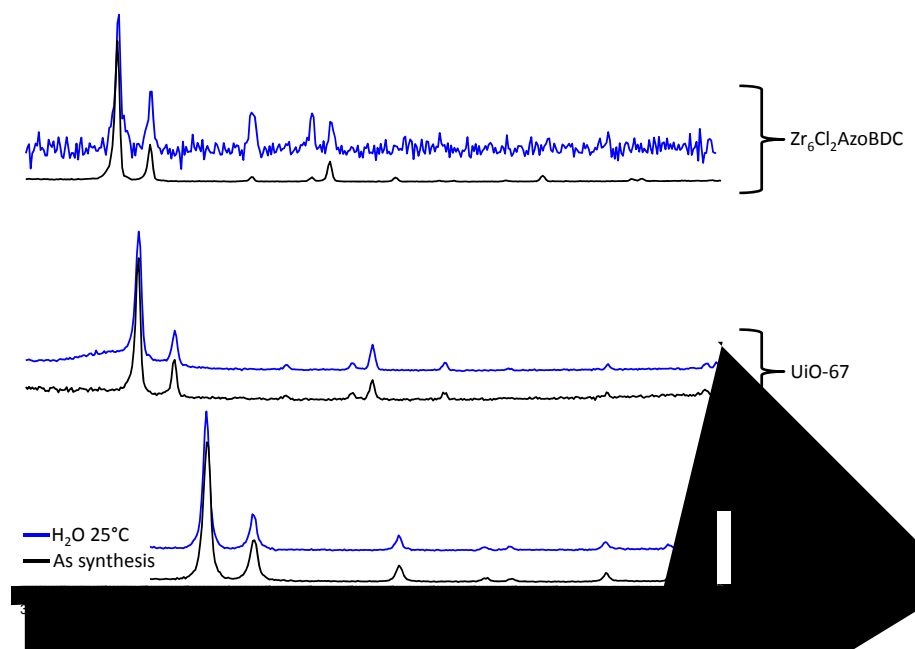


Fig. S6. XRPD diffractograms of UiO-66, UiO-67 and Zr₆-Cl₂AzoBDC (from bottom to top) ($\lambda Cu=1.5406\text{\AA}$). Before water treatment (black), after water treatment (25°C, 24 hours; in blue).

5. Mechanical pressure stability tests

The effect of pressure has been studied on some of the investigated Zr-MOFs including UiO-66, UiO-67 and $\text{Zr}_6\text{Cl}_2\text{AzoBDC}$ (Fig. S7). An increasing uniaxial compression has been applied on 10 mg of sample using an IR press and the integrity of their structure checked by XRPD. The structure is remained at moderate pressure, before a decrease of the crystallinity at much higher pressures (7.5 and 10 tons. cm^{-2}).

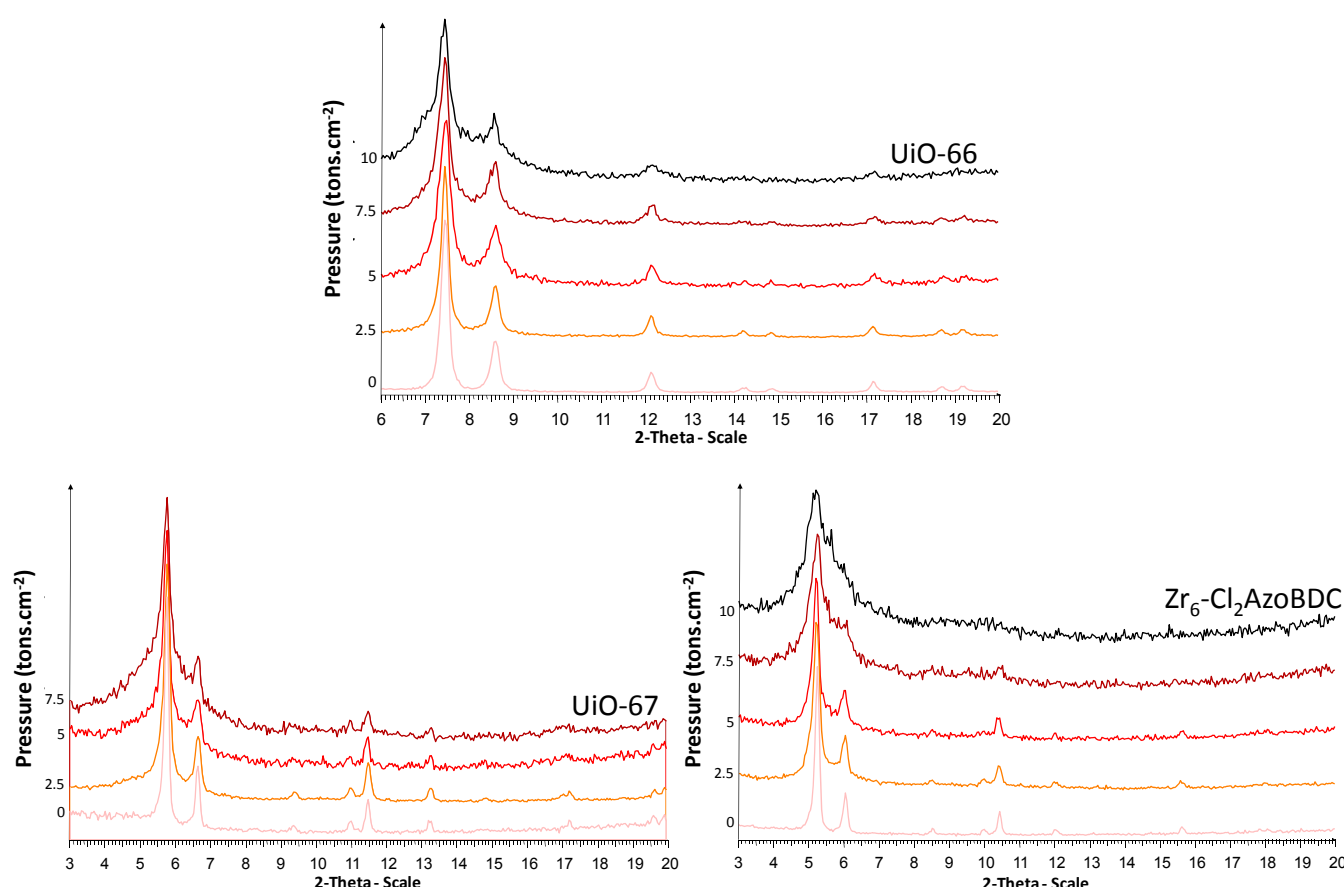


Fig. S7. Evolution of the XRPD diffractograms of UiO-66 , UiO-67 and $\text{Zr}_6\text{Cl}_2\text{AzoBDC}$ versus the applied mechanical pressure

The data are not reported for the $\text{Zr}_6\text{Cl}_2\text{AzoBDC}$ as this sample shows the same mechanical behavior than its non modified form.

6. High pressure adsorption of CO_2 and CH_4 on $\text{UiO-66}(\text{Zr})$

The excess adsorption isotherms for pure CO_2 and CH_4 were obtained gravimetrically using a commercial device (Rubotherm Präzisionsmeßtechnik GmbH). Approximately 1g of sample was used for these

experiments. Prior to each experiment the sample was activated *in situ* by heating under vacuum to 250°C for 16 hours. The experiments were carried out at 303.15 ± 0.2 K up to a maximum pressure of 90 bar for CH₄ and 60 bar for CO₂. The gas was introduced using a step-by-step method and equilibrium was assumed to have been reached when the variation of weight remained below 30µg over a 15 minute interval. The volume of the sample was determined from a blank experiment with He and used to compensate for buoyancy using the gas density measured by the Rubotherm balance. Each experiment consisted of two adsorption-desorption cycles with a two hour vacuum in between to ensure complete regeneration and reproducibility. The high purity gases were obtained from Air Liquide: N55 quality (99.9995% purity) for CH₄ and N45 quality (99.995% purity) for CO₂.

The absolute amounts adsorbed were calculated from the excess amounts using the bulk gas density ρ_{gas} and the experimental (0.47 cm³/g) pore volume of the sample V_{pore} :

$$m_{\text{absolute}}^a = m_{\text{excess}}^a + \rho_{\text{gas}} V_{\text{pore}}$$

7. Structural determination by Molecular Mechanics and DFT calculations

In this study, the crystalline structure of UiO-66 optimized by DFT calculation was directly adopted from our previous study.² Based on this parent structure of UiO-66, the starting configurations for the three extended Zr-MOFs (UiO-67, Zr-AzoBDC, Zr-Cl₂AzoBDC) were built by: (i) substituting the BDC ligands with the specific organic ligands, (ii) imposing the unit cell parameters determined from the X-ray powder diffraction experiment (XRPD); (iii) as done for the structures of UiO-66^{3,4} and UiO-67⁵ in previous works, changing the experimental space group of UiO-68 into F-43m, while changing those of the UiO-67, Zr₆-AzoBDC and Zr₆-Cl₂AzoBDC into F23 as discussed above. Regarding the UiO-68, we followed the same substitution strategy and we imposed the unit cell parameters taken from the literature on the UiO-68(NH₂) as starting point.⁶ Molecular mechanics approach was first employed to fully optimize these initial models using the Forceite module implemented in Materials Studio software, based on the Universal force field (UFF)⁷ and the charges calculated via the charge equilibration method developed by Rappé *et al.*⁸ Periodic DFT geometry optimization procedure based on the hybrid B3LYP

functional was further employed to refine these structures using the CRYSTAL09 code,⁹ where both cell parameters and atomic positions were allowed to fully relax. In these calculations, all electron basis sets were used for Zr, O, C, N, Cl and H atoms, where Basis sets for Zr and O were taken from Refs. 10 and 11 respectively whereas for C, N, Cl and H standard 6-31G(d,p) basis sets from Pople's family were adopted.¹² For the numerical integration of the exchange–correlation term, extra large grid (XLGRID) in a Lebedev scheme were used, which corresponds to a pruned grid with 75 radial points and 974 angular points in the region of chemical interest. The condition for the SCF convergence was set to 10^{-10} Hartrees during geometry optimization. The Pack–Monkhorst/Gilat shrinking factors for the reciprocal space were set to 2. The five truncation criteria (TOLINTEG) for the bielectronic integrals (Coulomb and HF exchange series) were set to 7 7 7 7 16. A modified Broyden scheme^{13a} following the method proposed by Johnson^{13b} was utilized to accelerate the convergence in the self-consistent calculations after five SCF iterations, with 50% of Fock/KS matrices simple mixing and with the Johnson parameter set to 0.05. This DFT computational strategy has been successfully employed to optimize the structures of UiO-66.³ The optimized crystalline structures and their structural features are shown in Fig. S8 and Table S3.

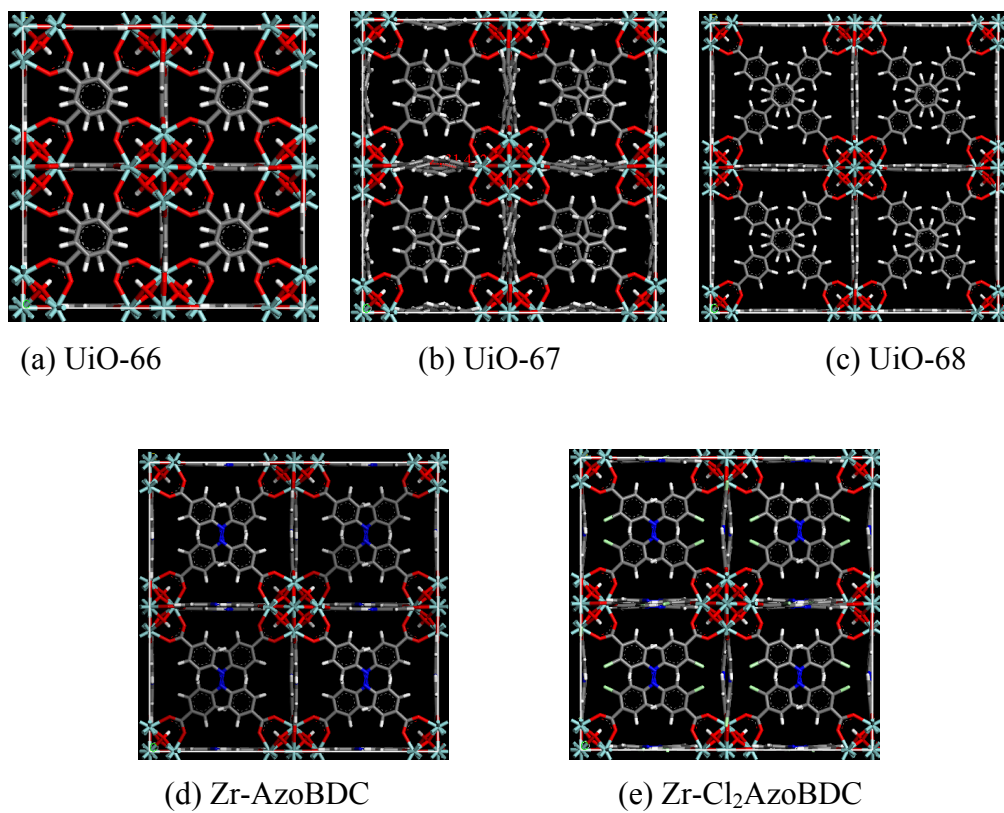


Fig. S8. Crystal structures of the extended Zr-MOF series determined by density functional theory (DFT) geometry optimization.

Table S3. Structural features of the extended Zr-MOF series.

Materials	Lattice sizes ^a (Å)	Lattice sizes ^b (Å)	ρ_{crys} ^b (g cm ⁻³)	V_{pore} ^c (cm ³ g ⁻¹)	S_{acc} ^c (m ² g ⁻¹)	$V_{\text{pore}}(\text{exp})$ (cm ³ g ⁻¹)	S_{BET} ^e (m ² g ⁻¹)
UiO-66	20.7430	20.7937	1.197	0.45	1018	0.47	1144
UiO-67	26.8780	27.0942	0.708	1.05	3071	0.69	1575
UiO-68	32.7767 ^d	33.3310	0.462	1.82	4239	Not reported	Not reported
Zr ₆ -AzoBDC	29.2400	29.8623	0.571	1.38	3642	0.51	1246
Zr ₆ -Cl ₂ AzoBDC	29.5710	29.9110	0.568	1.13	2885	0.94	2226

^a Obtained from the XRPD data obtained in this paper except for UiO-68 (taken from Ref. 6);

^b Obtained from the structures optimized by DFT calculations;

^c Theoretical calculations;

^d Obtained from the XRPD data for UiO-68-NH₂.⁶

^e Calculated from experimental N₂ sorption isotherms at 77K (Fig. S9)

8. Pore volume and accessible area calculations

The pore volumes (V_{pore}) of the adsorbents presented in Table S1 were obtained according to the thermodynamic method proposed by Myers and Monson.¹⁴ For the Zr-based MOFs series considered in this work, the Universal force field (UFF)⁷ was used to describe the Lennard-Jones (LJ) interactions of the framework atoms while the LJ parameters for Helium ($\epsilon/k_B = 10.9 \text{ K}$, $\sigma = 2.640 \text{ \AA}$) were taken from the work of Talu and Myers.¹⁵ The accessible surface area (S_{acc}) is purely based on the geometric topology of the adsorbent and calculated from a simple Monte Carlo integration technique where the center of mass of the probe molecule with hard sphere is “rolled” over the framework surface.¹⁶ In this method, a nitrogen-sized (3.6 Å) probe molecule is randomly inserted around each framework atom of the adsorbent and the fraction of the probe molecules without overlapping with the other framework atoms is then used to calculate the accessible surface area. The LJ size parameters of the framework atoms were the same as those used for the calculations of the pore volume. These calculations are presented in Table S3.

The BET surface areas have been further determined from the N₂ adsorption isotherms obtained at 77 K (see Figure S9) for the different UiOs.

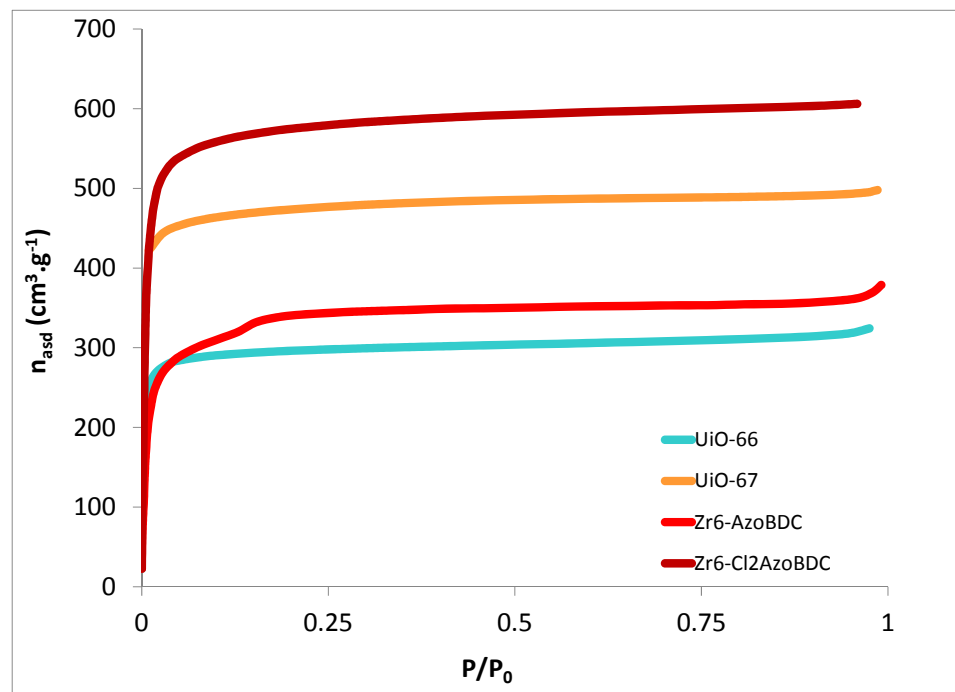


Fig. S9. Experimental nitrogen adsorption isotherms of UiO solids at 77K ($P_0=1 \text{ atm.}$).

The relatively low surface area for Zr_6AzoBDC compared to $\text{Zr}_6\text{Cl}_2\text{AzoBDC}$ might be explained by the higher amount of free acid in the cavities of the as-synthesized structure (IR spectroscopy, $\nu_{\text{C=O}}=1683\text{cm}^{-1}$) compared to the chlorinated version, as shown on Fig. S10. That makes the MOF much more difficult to activate completely.

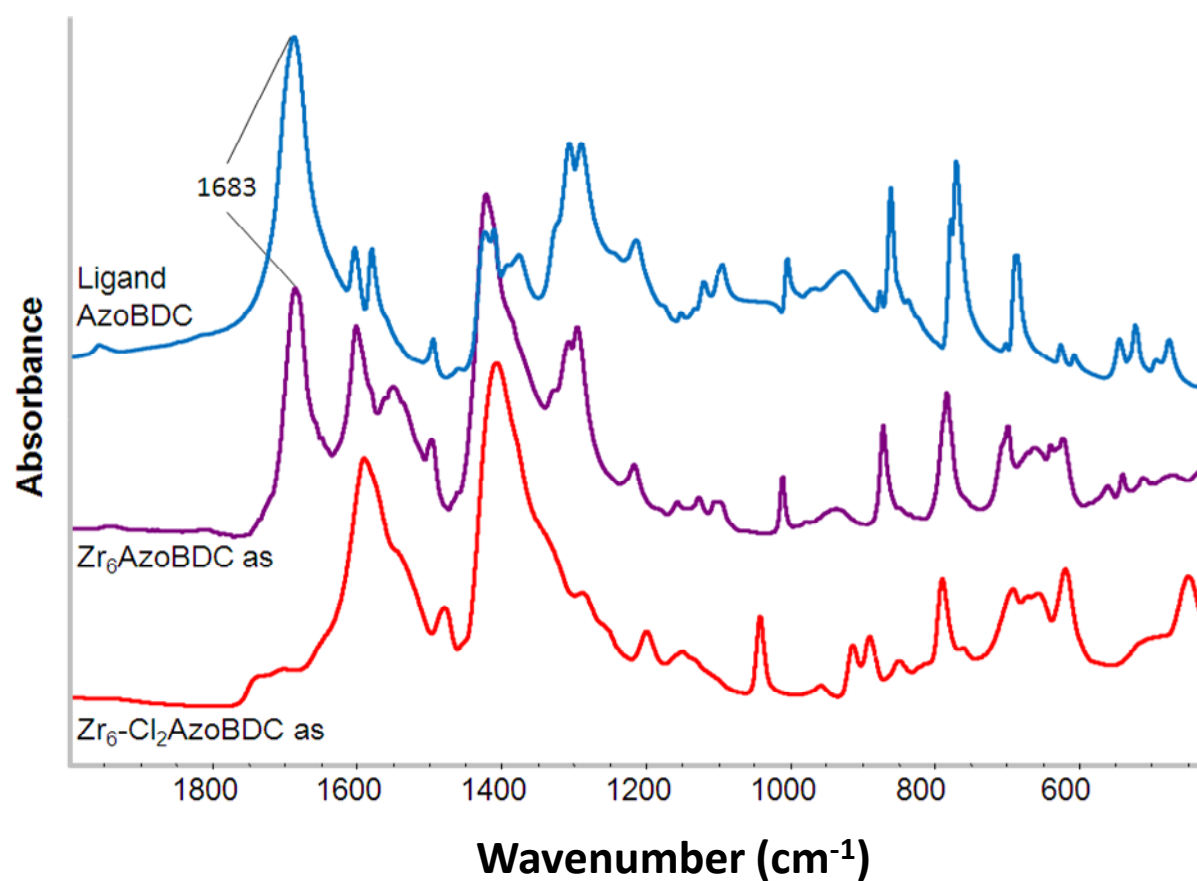


Fig. S10. Infrared spectra of the as synthesized $\text{Zr}_6\text{-AzoBDC}$ (purple), $\text{Zr}_6\text{-Cl}_2\text{AzoBDC}$ (red) and the AzoBDC ligand (blue)

9. Atomic partial Charge calculations

Due to the large quadruple moment of CO₂ molecule, many studies have demonstrated that it is very important to take the CO₂-MOF electrostatic interactions into account.¹⁷ In this work, density functional theory calculations were performed on the clusters cleaved from the optimized unit cell of each Zr-based MOF structure. These clusters include building units (e.g. metal-oxide corner and linker) representative of their respective unit cells. All the terminations were saturated by methyl groups with standard sp³ geometry. The electrostatic potential (ESP) charges obtained with ChelpG method were used as the atomic partial charges, which has been recognized as the most popular and reliable electrostatic charge calculation method.¹⁸ To that purpose, the density functional theory calculations were carried out by means of the GAUSSIAN03 program¹⁹ using the Perdew-Burke-Ernzerhof (PBE) exchange and correlation functional. For all these calculations, the basis set LANL2DZ was used for atom Zr, while 6-31+G* was employed for the rest of the atoms which includes one diffuse and one polarization function on atoms heavier than He. For heavy atoms, effective core potential (ECP) is often chosen in ab initio calculations to reduce the amount of the necessary computation. LANL2DZ is a collection of double- ζ basis sets, which is one of the most common ECP basis sets for complexes involving transition metal elements.²⁰ In these DFT calculations, the atomic van der Waals (vdW) radii for the framework nonmetal elements used to fit the ESP charges were taken from the work of Bondi *et al.*²¹ As the metal atom Zr was not treated by Bondi, the vdW radius of it was assigned to be 0.75 Å larger than its covalent radius according to the Pauling's approximation used in the Bondi's article. The covalent radius of this element was adopted from the work of Cordero *et al.*²² This method has been employed previously to estimate the ESP charges and binding energies in many MOFs including UiO-66.^{Error! Reference source not found.,4} The cleaved clusters with the location of atomic types and resulting charges are shown in Figures S11-S15 and listed in Tables S4-S8 respectively, where the corresponding results for the UiO-66 were obtained in our previous work.⁴

9.1 Model cluster and atomic partial charges of UiO-66

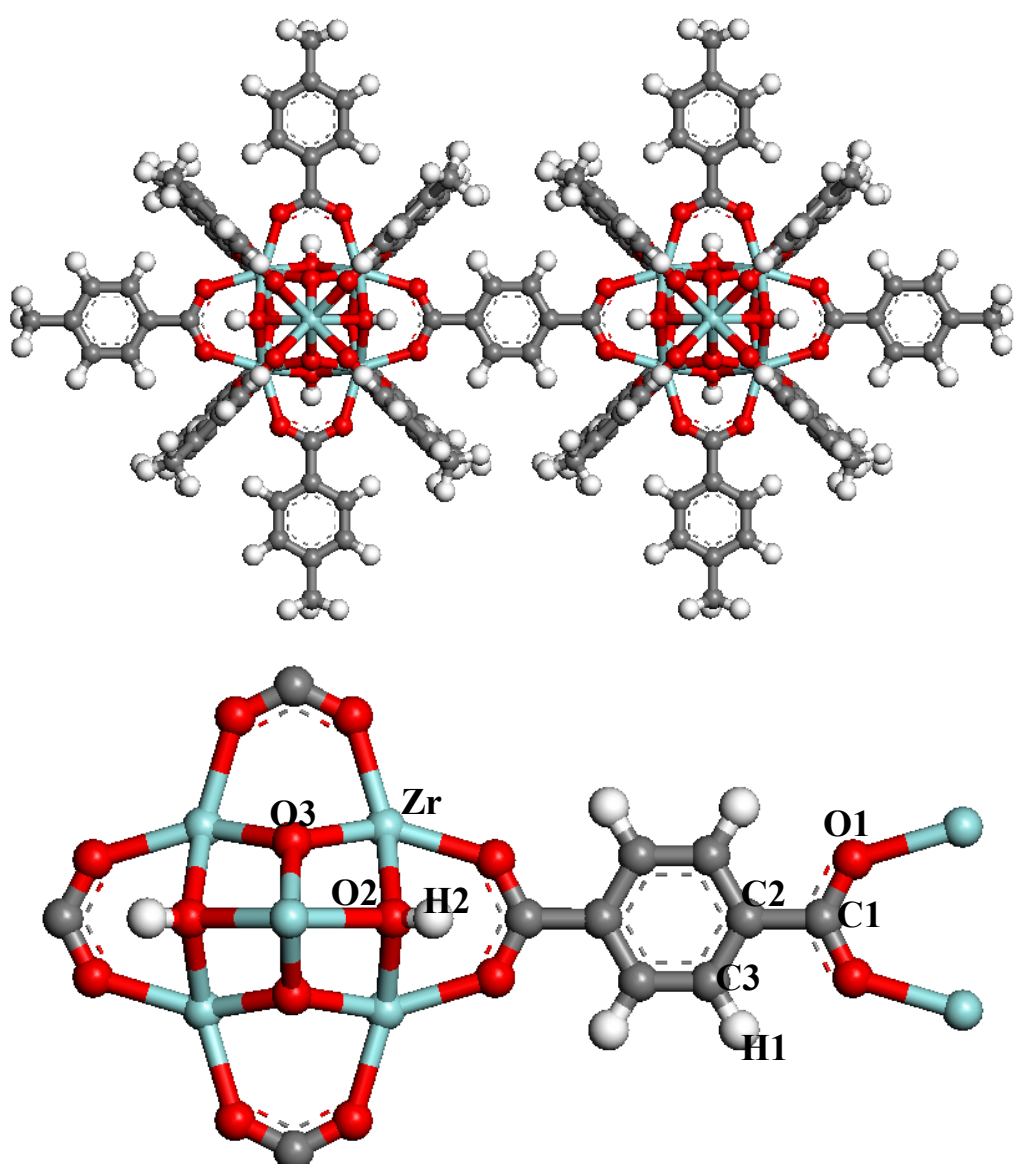


Fig. S11. Cluster used for calculating the partial charges for each atom of the UiO-66 form. The terminations of the cluster were saturated with methyl groups to minimize the boundary effects.

Table S4. Atomic partial charges for the UiO-66 structure derived on DFT/PBE Level.

Atomic types	Zr	O1	O2	O3	C1	C2	C3	H1	H2
Charge (e)	2.008	-0.582	-1.179	-0.741	0.625	-0.002	-0.121	0.127	0.495

9.2 Model cluster and atomic partial charges of UiO-67

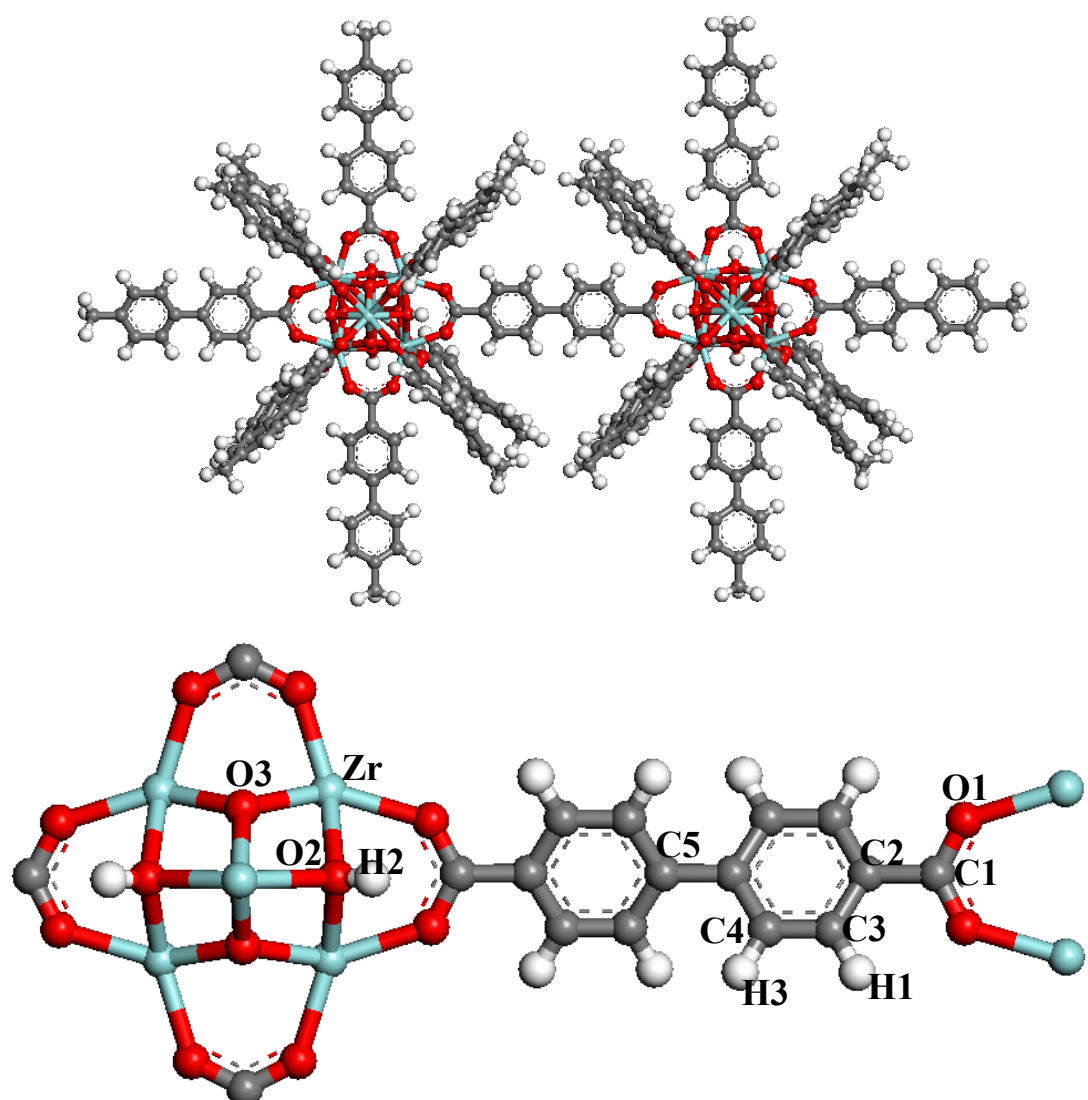


Fig. S12. Cluster used for calculating partial charges on UiO-67 atoms. The terminations of the cluster were saturated with methyl groups to minimize the boundary effects.

Table S5. Atomic partial charges for the UiO-67 structure derived on DFT/PBE Level.

Atomic types	Zr	O1	O2	O3	C1	C2	C3	C4
Charge (e)	1.876	-0.610	-0.990	-0.723	0.678	-0.011	-0.134	-0.138
Atomic types	C5	H1	H2	H3				
Charge (e)	0.072	0.135	0.450	0.119				

9.3 Model cluster and atomic partial charges of UiO-68

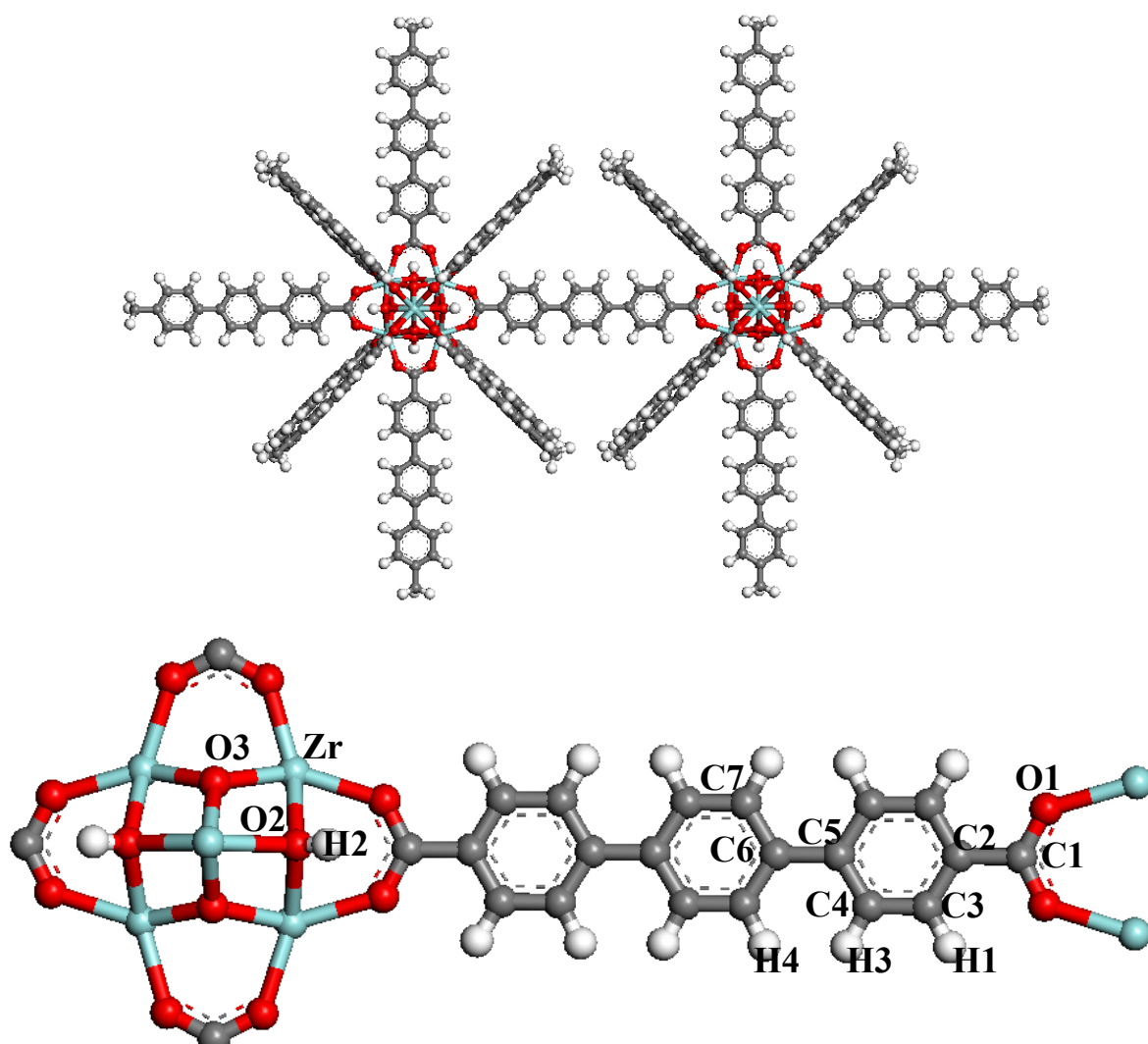


Fig. S13 Cluster used for calculating partial charges on UiO-68 atoms. The terminations of the cluster were saturated with methyl groups to minimize the boundary effects.

Table S6. Atomic partial charges for the UiO-68 structure derived on DFT/PBE Level.

Atomic types	Zr	O1	O2	O3	C1	C2	C3	C4	C5
Charge (e)	1.946	-0.589	-1.076	-0.728	0.630	0.006	-0.126	-0.168	0.089
Charge (e)	0.073	-0.155	0.126	0.475	0.126	0.122			

9.4 Model cluster and atomic partial charges of Zr-AzoBDC

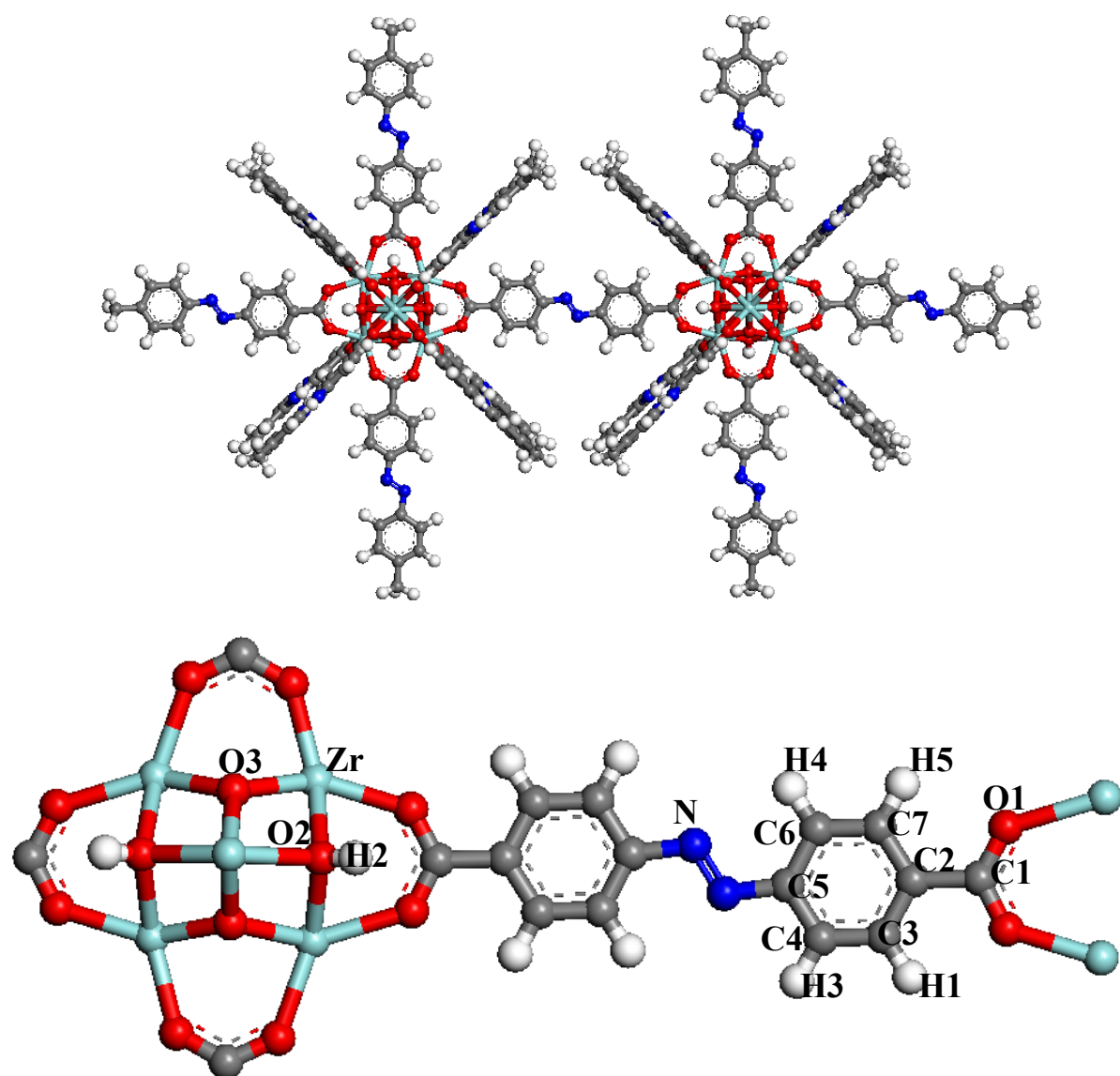


Fig. S14. Cluster used for calculating partial charges on Zr-AzoBDC atoms. The terminations of the cluster were saturated with methyl groups to minimize the boundary effects.

Table S7. Atomic partial charges for the Zr-AzoBDC structure derived on DFT/PBE Level.

Atomic types	Zr	O1	O2	O3	C1	C2	C3	C4	C5
Charge (e)	2.180	-0.642	-1.123	-0.908	0.782	-0.197	0.046	-0.354	0.459
Atomic types	C6	C7	H1	H2	H3	H4	H5	N	
Charge (e)	-0.159	-0.083	0.118	0.465	0.139	0.074	0.135	-0.244	

9.5 Model cluster and atomic partial charges of Zr-Cl₂AzoBDC

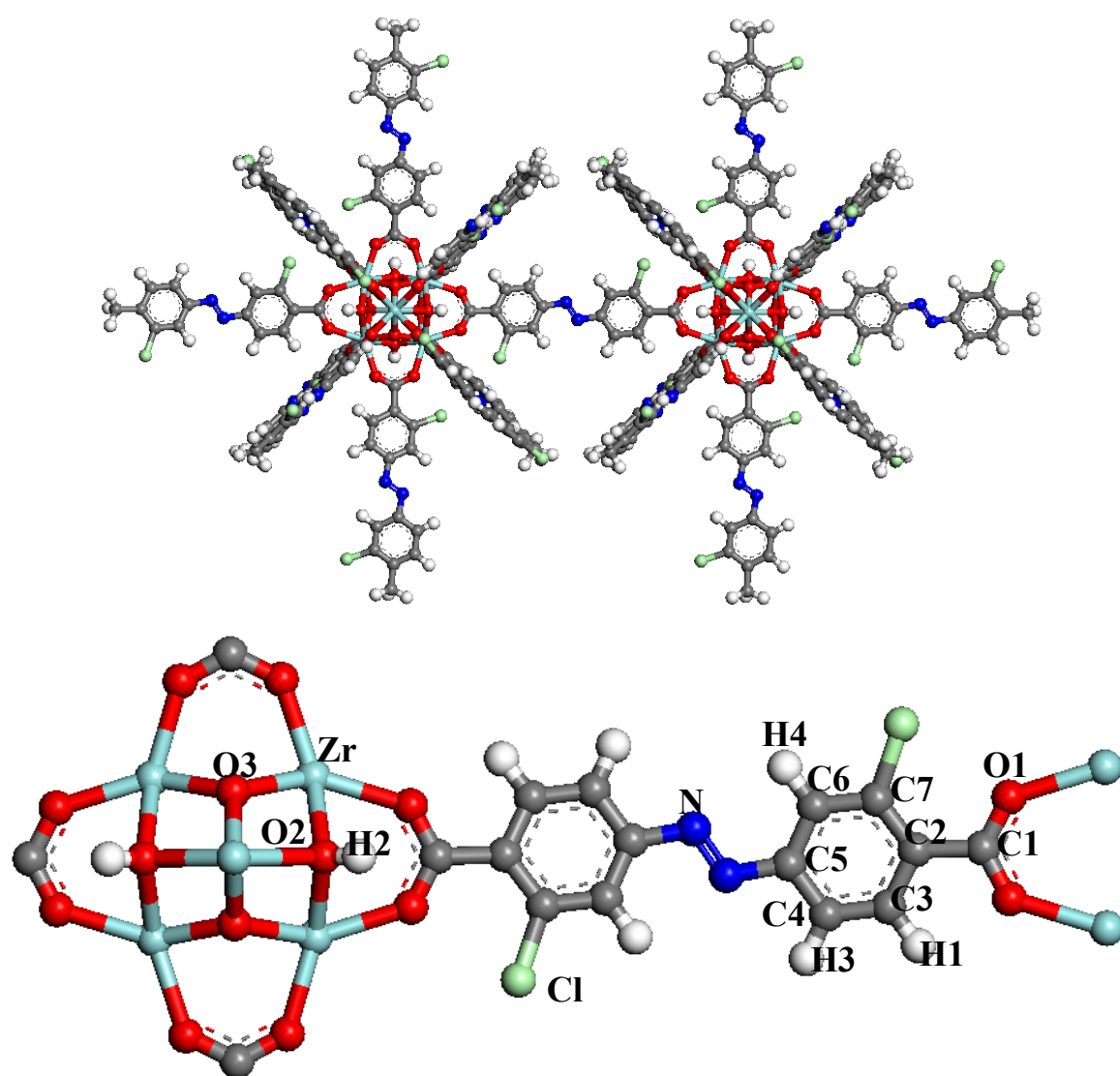


Fig. S15. Cluster used for calculating partial charges on Zr-Cl₂AzoBDC atoms. The terminations of the cluster were saturated with methyl groups to minimize the boundary effects.

Table S8. Atomic partial charges for the Zr-Cl₂AzoBDC structure derived on DFT/PBE Level.

Atomic types	Zr	O1	O2	O3	C1	C2	C3	C4	C5
Charge (e)	2.274	-0.689	-1.126	-0.963	0.755	-0.133	-0.043	-0.317	0.393
Atomic types	C6	C7	H1	H2	H3	H4	Cl	N	
Charge (e)	-0.119	0.070	0.157	0.466	0.140	0.051	-0.066	-0.201	

10. Interatomic Potentials

Successful investigation of the adsorption/diffusion behavior of fluid in MOFs requires an accurate description of the interactions between adsorbate-adsorbate and adsorbate-MOF. In this present work, a single LJ interaction site model was used to describe a CH₄ molecule with potential parameters taken from the TraPPE forcefield.²³Error! Reference source not found.^a The CO₂ molecule was represented by the conventional rigid linear triatomic model with three charged LJ interaction sites (C–O bond length of 1.149 Å) located on each atom as previously described by Harris and Yung.^{23b} All the corresponding atomic partial charges and interatomic potential parameters are reported in Table S9. The interactions between CO₂ and the surface of the Zr-MOFs were described by a combination of site-site LJ and Coulombic potentials, while the interactions between CH₄ and Zr-MOF series were only treated using a site-site LJ potential. The LJ potential parameters for the framework atoms of MOFs studied in these work were taken from DREIDING²⁴ and UFF⁷ force fields for CH₄ and CO₂ respectively, as given in Table S10. All the LJ cross interaction parameters including adsorbate/adsorbate and adsorbate/MOF were determined by the Lorentz-Berthelot mixing rule. The above set of force fields has been validated in our previous studies for the dehydroxylated² and hydroxylated UiO-66⁴²² as well as its hydroxylated form with amine modification,Error! Reference source not found. where both the simulated isotherms and low-coverage adsorption enthalpies of CH₄ and CO₂ were in good agreement with the gravimetric and calorimetric measurements. Thus, to be consistent, the same force fields were also adopted in current work. Actually, when one deals with the adsorption of CH₄ or alkanes in MOF materials, one can find in the literature that the description of the framework via the DREIDING forcefield usually leads to a better agreement with the experimental results.²⁵ Similar observations were also found that the simulations with UFF force field lead to a better agreement with the experimental data on the CO₂ adsorption in various MOFs.²⁶

Table S9. Potential parameters and partial charges for the adsorbates

Atomic type	σ (Å)	ε / k_B (K)	q (e)
CH ₄	3.730	148.000	0.0000
CO ₂ _C	2.757	28.129	0.6512
CO ₂ _O	3.033	80.507	-0.3256

Table S10. LJ potential parameters for the atoms of the Zr-MOF series.

Elements	DREIDING		UFF	
	σ (Å)	ε / k_B (K)	σ (Å)	ε / k_B (K)
Zr	2.783 ^a	34.724 ^a	2.783	34.724
C	3.473	47.859	3.431	52.841
O	3.033	48.161	3.118	30.195
H	2.846	7.649	2.571	22.143
N	3.263	38.951	3.261	34.724
Cl	3.519	142.570	3.516	114.237

^a taken from UFF.

11. Details of the molecular Simulations

Grand canonical Monte Carlo (GCMC) simulations were performed to investigate the adsorption of CO₂ and CH₄ gases in the MOFs at 303 K, using our newly developed simulation code CADSS (Complex Adsorption and Diffusion Simulation Suite). In our simulations, molecules involve four types of trials: attempts (i) to displace a molecule (translation or rotation), (ii) to create a new molecule, and (iii) to delete an existing molecule. Details on the method can be found elsewhere.²⁷ The simulation box consisted of 8 (2×2×2) primitive cells for each Zr-MOF. A cutoff radius of 14.0 Å was applied to the Lennard-Jones (LJ) interactions, while the long-range electrostatic interactions were handled by the Ewald summation technique. Periodic boundary conditions were considered in all three dimensions. Peng-Robinson equation of state was used to convert the pressure to the corresponding fugacity used in the GCMC simulations. As the adsorbents were maintained fixed during the simulations, the potential energies between an adsorbate and the adsorbent were initially tabulated on a series of three-dimensional grid points with grid spacing 0.15 Å. During the simulations, the potential energy at any position of the

adsorbent was determined by interpolation. For each state point, GCMC simulations consisted of 2×10^7 steps to ensure the equilibration, followed by 2×10^7 steps to sample the desired thermodynamic properties. For the calculation of the adsorption enthalpies (ΔH) of CH₄ and CO₂ at the limit of zero coverage, configurational-bias Monte Carlo simulations in the canonical (NVT) ensemble were further performed using the revised Widom's test particle method.²⁸

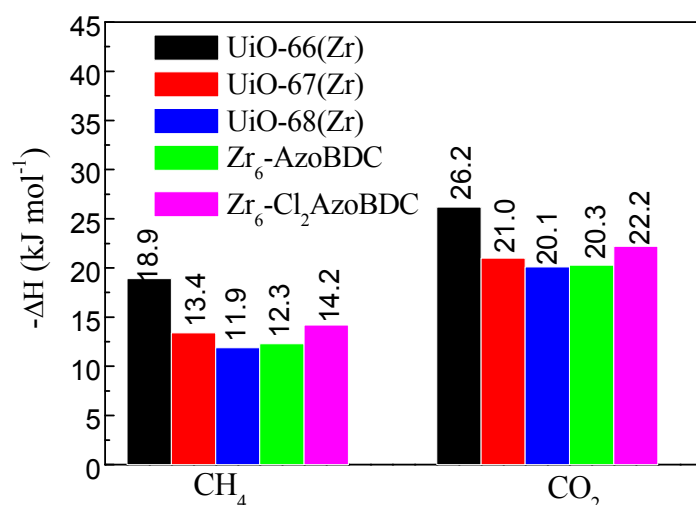


Fig. S16 Calculated low-coverage adsorption enthalpies of pure CH₄ and CO₂ gases in the Zr-MOFs at 303 K.

References:

1. (a) S. Ameerunisha, P.S. Zacharias, *J.Chem.Soc.Perkin.Trans 2*, 1995, 1679; (b) A. Schaate, S. Dühnen, G. Platz, S. Lilienthal, A. M. Schneider and P. Behrens, *Eur. J. Inorg. Chem.*, 2012, **5**, 790; P. S. Mukherjee, N. Das, Y. K. Kryschchenko, A. M. Arif and P. J. Stang, *J. Am. Chem. Soc.* 2004, **126**, 2464.
2. Q. Yang, A. D. Wiersum, H. Jobic, V. Guillerm, C. Serre, P. L. Llewellyn, G. Maurin, *J. Phys. Chem. C*, 2011, **115**, 13768.
3. L. Valenzano, B. Civalleri, S. Chavan, S. Bordiga, M. H. Nilsen, S. Jakobsen, K. P. Lillerud, C. Lamberti, *Chem. Mater.*, 2011, **23**, 1700.
4. Q. Yang, A. D. Wiersum, P. L. Llewellyn, V. Guillerm, C. Serre, G. Maurin, *Chem. Commun.*, 2011, **47**, 9603.

5. S. Chavan, J. G. Vitillo, D. Gianolio, O. Zavorotynska, B. Civalleri, S. Jakobsen, M. H. Nilsen, L. Valenzano, C. Lamberti, K. P. Lillerud and S. Bordiga, *Phys. Chem. Chem. Phys.*, 2012, **12**, 1614.
6. A. Schaate, P. Roy, A. Godt, J. Lippke, F. Waltz, M. Wiebcke and P. Behrens, *Chem.-Eur. J.*, 2011, **17**, 6643.
7. A. K. Rappé, C. J. Casewit, K. S. Colwell, W. A. Goddard III and W. M. Skiff, *J. Am. Chem. Soc.*, 1992, **114**, 10024.
8. A.K. Rappé, W.A. Goddard III, *J. Phys. Chem.*, 1991, **95**, 3358.
9. R. Dovesi, V. R. Saunders, R. Roetti, R. Orlando, C. M. Zicovich-Wilson, F. Pascale, B. Civalleri, K. Doll, N. M. Harrison, I. J. Bush, P. D'Arco and M. Llunell, CRYSTAL09, University of Torino, Torino, 2009.
10. http://www.crystal.unito.it/Basis_Sets/zirconium.html.
11. Y. Noel, C. M. Zicovich-Wilson, B. Civalleri, P. D'Arco and R. Dovesi, *Phys. Rev. B: Condens. Matter*, 2002, **65**, 014111.
12. <https://bse.pnl.gov/bse/portal>.
13. (a) C. G. Broyden, *Math. Comput. Modell.*, 1965, **19**, 577; (b) D. D. Johnson, *Phys. Rev. B*, 1988, **38**, 12807.
14. A. L. Myers and P. A. Monson, *Langmuir*, 2002, **18**, 10261.
15. O. Talu and A. L. Myers, *AICHE J.*, 2001, **47**, 1160.
16. T. Düren, F. Millange, G. Férey, K. S. Walton and R. Q. Snurr, *J. Phys. Chem. C*, 2007, **111**, 15350.
17. (a) Y.-S. Bae, K.L. Mulfort, H. Frost, P. Ryan, S. Punnathanam, L.J. Broadbelt, J.T. Hupp, R.Q. Snurr, *Langmuir*, 2008, **24**, 8592; (b) Q. Yang and C. Zhong, *ChemPhysChem*, 2006, **7**, 1417.
18. (a) H. Heinz and U. W. Suter, *J. Phys. Chem. B*, 2004, **108**, 18341; (b) G. S. Maciel and E. Garcia, *Chem. Phys. Lett.*, 2005, **409**, 29.
19. M. J. Frisch, G. W. Trucks, H. B. Schlegel, G. E. Scuseria, M. A. Robb, J. R. Cheeseman, J. A. Montgomery, Jr., T. Vreven, K. N. Kudin, J. C. Burant, J. M. Millam, S. S. Iyengar, J. Tomasi, V. Barone, B. Mennucci, M. Cossi, G. Scalmani, N. Rega, G. A. Petersson, H. Nakatsuji, M. Hada, M. Ehara, K. Toyota, R. Fukuda, J. Hasegawa, M. Ishida, T. Nakajima, Y. Honda, O. Kitao, H. Nakai, M. Klene, X. Li, J. E. Knox, H. P. Hratchian, J. B. Cross, V. Bakken, C. Adamo, J. Jaramillo, R. Gomperts, R. E. Stratmann, O. Yazyev, A. J. Austin, R. Cammi, C. Pomelli, J. W. Ochterski, P. Y. Ayala, K. Morokuma, G. A. Voth, P. Salvador, J. J. Dannenberg, V. G. Zakrzewski, S. Dapprich, A. D. Daniels, M. C. Strain, O. Farkas, D. K. Malick, A. D. Rabuck, K. Raghavachari, J. B. Foresman, J. V. Ortiz, Q. Cui, A. G. Baboul, S. Clifford, J. Cioslowski, B. B. Stefanov, G. Liu, A. Liashenko, P. Piskorz, I. Komaromi, R. L. Martin, D. J. Fox, T. Keith, M. A. Al-Laham, C. Y. Peng, A. Nanayakkara, M. Challacombe, P. M. W. Gill, B. Johnson, W. Chen, M. W. Wong, C. Gonzalez, and J. A. Pople, *GAUSSIAN 03*, Revision E.01, Gaussian, Inc., Wallingford CT, 2004.

20. (a) D. Foguet-Albiol, T. A. O'Brien, W. Wernsdorfer, B. Moulton, M. J. Zaworotko, K. A. Abbound and G. Christou, *Angew. Chem., Int. Ed.*, 2005, **44**, 897; (b) E. R. Davidson and A. E. Clark, *J. Phys. Chem. A*, 2002, **106**, 7456.
21. A. Bondi, *J. Phys. Chem.*, 1964, **68**, 441.
22. B. Cordero, V. Gomez, A. E. Platero-Prats, M. Reves, J. Echeverria, E. Cremades, F. Barragan and S. Alvarez, *Dalton Trans.*, 2008, **21**, 2832.
23. (a) M. G. Martin and J. I. Siepmann, *J. Phys. Chem. B*, 1998, **102**, 2569; (b) J. G. Harris and K. Hung, *J. Phys. Chem.*, 1995, **99**, 12021.
24. S. L. Mayo, B. D. Olafson and W. A. Goddard III, *J. Phys. Chem.*, 1990, **94**, 8897.
25. (a) T. Duren and R. Q. Snurr, *J. Phys. Chem. B* **2004**, *108*, 15703; (b) V. Finsy, S. Calero, E. García-Pérez, P. J. Merkling, G. Vedts, D. E. De Vos, G. V. Baron and L. F. M. Denayer, *Phys. Chem. Chem. Phys.* **2009**, *11*, 3515.
26. (a) W. Morris, B. Leung, H. Furukawa, O. K. Yaghi, N. He, H. Hayashi, Y. Hounodonougbo, M. Asta, B. B. Laird and O. M. Yaghi, *J. Am. Chem. Soc.*, 2010, **132**, 11006; (b) A. Sirjoos Singh, S. Alavi and T. K. Woo, *J. Phys. Chem. C*, 2010, **114**, 2171; (c) R. Babarao and J. W. Jiang, *Langmuir*, 2008, **24**, 6270.
27. Q. Yang and C. Zhong, *J. Phys. Chem. B*, 2006, **110**, 17776.
28. T. J. H. Vlugt, E. García-Pérez, D. Dubbeldam, S. Ban and S. Calero, *J. Chem. Theory Comput.*, 2008, **4**, 1107.